MATEC Web of Conferences **14**, 16004 (2014)
DOI: 10.1051/matecconf/20141416004

Simulation of oxidation-nitridation-induced microstructural degradation in a cracked Ni-based superalloy at high temperature

Kang Yuan[1,a], Ru Lin Peng[1], Xin-Hai Li[2], Sten Johansson[1], and Yan-Dong Wang[3]

[1] Department of Management and Engineering, Linköping University, 58183 Linkoping, Sweden
[2] Siemens Industrial Turbomachinery AB, 61283 Finspong, Sweden
[3] University of Science and Technology Beijing, Beijing 100083, China

Abstract. In turbine engines, high temperature components made of superalloys may crack in a creep process during service. With the inward flux of the gases, e.g. oxygen and nitrogen, along those cracks, the microstructure of the superalloy substrate nearby the cracks may degrade by internal oxidation and nitridation. The aim of this study is to investigate and simulate the oxidation-nitridation-induced microstructural degradation in superalloys by taking a variant of Ni-based superalloy IN-792 as a sample. After the creep testing of the superalloy in air, the microstructures on the cross section of the superalloy were analysed in a scanning electron microscope, equipped with energy/wavelength dispersive systems. Internal oxidation and nitridation, presenting by Al/Ti oxides and nitrides, were observed under a porous and even cracked Cr-oxide scale which was formed on the superalloy surface or along the creep cracks connecting the superalloy surface. Meanwhile, the reinforcing γ' precipitates were depleted. Such oxidation-nitridation-induced microstructural degradation was simulated by using an oxidation-diffusion model, focusing the diffusion of the alloying elements in metallic phases of the superalloy.

1. Introduction

Superalloys are widely used to sustain creep and fatigue loadings in gas turbine engines at high temperature in harsh environment. Most superalloys can not form a dense and protective oxide layer at high temperature so the inner microstructure of the superalloy, typically consisting of γ/γ' phases, will be degraded due to internal oxidation and nitridation [1–3]. The degradation of the microstructure can happen near the superalloy surface or along a surface-connecting crack.

The diffusion of oxygen and nitrogen in the superalloy cause the formation of internal oxides and nitrides. Common oxides/nitrides in superalloys are, for instance, alumina, AlN and TiN [2,3]. The penetration depths of the oxides and nitrides are thermodynamically dependent upon the forming energy of the oxides/nitrides, and kinetically upon the solution and diffusivity of oxygen/nitrogen and the alloying elements in the material [3,4].

Many efforts have been taken to model the internal oxidation or nitridation in alloys. By applying Wagner's equations [5] for internal oxidation, U. Krupp et al. [6] simulated the development of internal nitridation in Ni-based alloys. A similar approach was also applied on some commercial superalloys [2]. Referencing those interesting researches, an oxidation-diffusion model by using DICTRA and Matlab software is developed in this paper to simulate the combined effect of external oxidation and internal oxidation/nitridation. By using this model, the alloying elemental diffusion and corresponding microstructural degradation in a Ni-based superalloy are predicted.

2. Experiments and simulation setting-up

The material used in this study was a Ni-based polycrystalline superalloy IN-792. After being made into a sheet sample (with 1 mm × 10 mm cross section), the superalloy was solution treated at 1120 ° C for 2 h, followed by 24-hour aging at 845 ° C and then cooling to room temperature by air.

The sheet sample was loaded under a constant tensile stress at 950 ° C in air to simulate the creep process. After fracture which occurred after 680 h, the fractured sample was cut in the load direction. The obtained length cross-section was then carefully polished to study the microstructures by scanning electron microscope (SEM). The composition of the superalloy from energy-dispersive X-ray spectroscopy (EDS) analysis, was Ni-9.03Co-12.4Cr-3.32Al-3.94Ti-4.68Ta-4.80W-2.06Mo by wt.% (Ni-9.08Co-14.13Cr-7.29Al-4.88Ti-1.53Ta-1.54W-1.27Mo by at.%). The composition was used as input for the oxidation-diffusion modelling. In this study wavelength-dispersive spectroscopy (WDS) was also utilized for a qualitative measurement of certain elements.

[a] Corresponding author: kang.yuan@liu.se

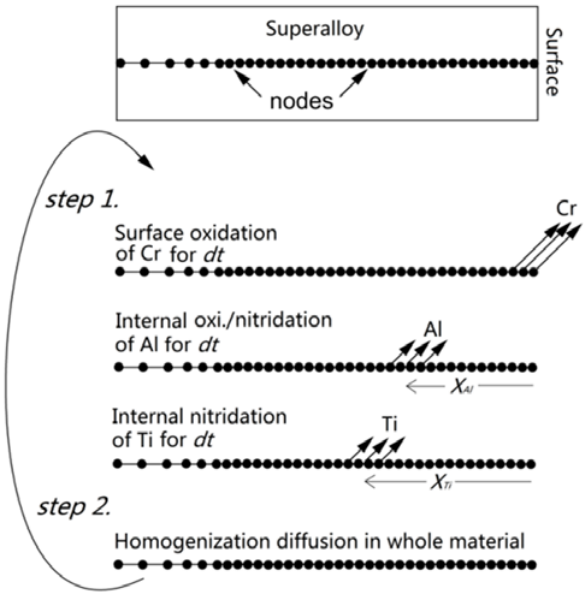

Figure 1. The oxidation-diffusion model. X denotes the penetration depth of the internal oxidation/nitridation.

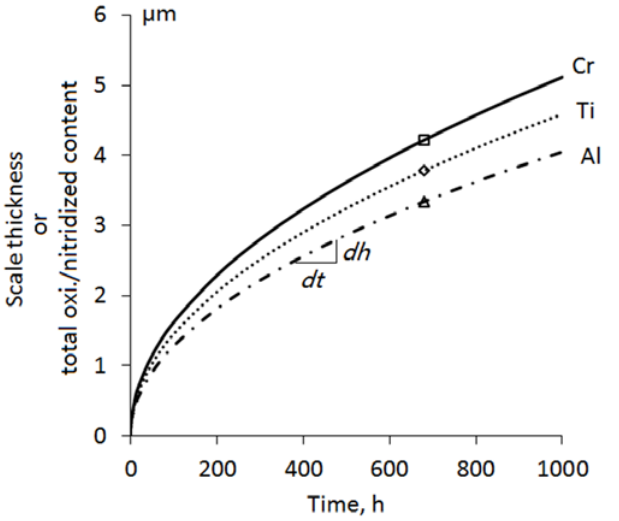

Figure 2. The fitted parabolic curves for the depletion of Cr, Ti and Al due to oxidation/nitridation. The points highlighted on the curves are from the image analysing on the EDS images in Fig. 6. The parabolic constants for Cr, Ti and Al are 0.0262 μm^2/h, 0.0210 μm^2/h, 0.0164 μm^2/h, respectively.

The oxidation-diffusion modelling of the superalloy was achieved by combining the software of DICTRA [7–9] and Matlab, with the Ni-based databases of TCNI5 and MOBNI2 [10]. The homogenization model of "rule of mixture" [11] was used to simulate the diffusion of alloying elements in the main metallic phases, FCC-γ and FCC-γ', of the alloy.

Based on experimental observations, surface oxidation of Cr, internal oxidation/nitridation of Al and internal nitridation of Ti were included in the model. As shown in Fig. 1, the modelling was an iterative process where each iteration involved two steps. In *step 1*, the internally oxidized and/or nitridized contents of Al and Ti, *dh,* during the iteration time, *dt*, was removed from the composition-stored nodes at the front of the penetration depths of the oxides or nitrides. The surface oxidation of Cr was performed in the outmost nodes. The oxidation and nitridation were assumed to start from the beginning of the creep testing. The rate of the depletion of Cr, Al and Ti was simply assumed to obey the parabolic law as shown in Fig. 2. The penetration rate of Al/Ti oxides/nitrides, $\frac{\partial X_{Al}}{\partial t}$ and $\frac{\partial X_{Ti}}{\partial t}$, can be also described by parabolic laws [3, 4]. With the modified composition profiles from *step 1*, diffusion by the homogenization model was run through the whole material in *step 2*. The updated composition profile after *step 2* is then used as input for the new iteration.

3. Results

3.1. Experimental results

Oxidation and nitridation in the superalloy are observed at the exposed surface and along the creep-induced cracks. Fig. 3 and Fig. 5 show typical microstructure and measured composition profiles near the superalloy surface and along the creep crack, respectively. The oxidation occurred at the superalloy surface is particularly named as the "surface oxidation"; the oxidation occurred along the creep crack is named as the "cracking oxidation". EDS mapping results of some elements are given in Fig. 4 and Fig. 6. The identification of the oxides and nitrides formed was mainly based on the EDS mapping results, but also checked by WDS as shown in Fig. 3b,c. WDS can be used to distinguish elements with energy peaks to close to be distinguished by EDS, for example N, Ti and Co [1]. WDS is also more powerful when detecting light elements, like oxygen and nitrogen. In this paper, the precipitates of oxides and nitrides are all checked by EDS and WDS. The quantitative EDS compositions have been normalized.

The outside oxide scale ("1" in Fig. 3a) on the surface of the superalloy is Cr-rich and is probably Cr_2O_3. Some other elements like Ti, Al, and Ni are also shown in the scale according to the EDS maps in Fig. 4; they may be dissolved in the Cr_2O_3 or to form other types of oxides. Under the Cr-rich scale, precipitates of Al_2O_3 ("2") can be seen in the superalloy matrix. TiN precipitates ("3") are formed in inner area and shown as needle-shape. In the internal oxidation/nitridation areas in Fig. 3a, the γ' phases are totally depleted. As the composition profiles shown (Fig. 3d), in the internal oxidation/nitridation areas some Al and Ti (also O and N) peaks can be found, corresponding to the formation of Al_2O_3 and TiN. Fig. 4 gives the EDS maps for Fig. 3a (in red square in Fig. 3a).

The internal oxidation and nitridation can be also found nearby the crack which is formed during the creep process and connected to the superalloy surface, as shown in Fig. 5a. The oxide in the crack is mainly Cr-oxides ("1"), followed by some internal oxide and nitride precipitates in the superalloy matrix, i.e. Al_2O_3 and AlN ("2") and TiN ("3"). "4" is for $\gamma + \gamma$'. Fig. 5b shows the corresponding composition profiles of Fig. 5a, and the EDS mapping results are in Fig. 6.

The microstructure and EDS maps in Figs. 7–9 show the degradation of γ' phases and the precipitation of

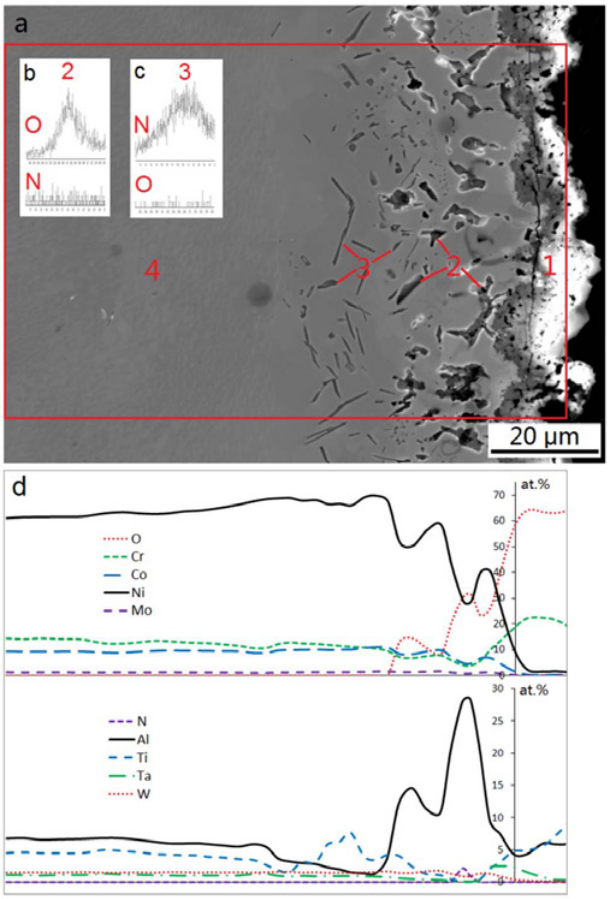

Figure 3. Surface oxidation. (a) A SEM image near the superalloy surface ("1" for surface oxides, Cr-rich, "2" for Al_2O_3, "3" for TiN, and "4" for $\gamma + \gamma'$). (b) oxygen and nitrogen peaks of the precipitates "2" in (a) by WDS. (c) oxygen and nitrogen peaks of the precipitates "3" in (a) by WDS. (d) The EDS composition profiles of elements in the red square in figure (a).

TiN due to the internal nitridation under the creep-crack. Feature "1" in Fig. 7 tracks the previous γ' phases which are around 1 μm. Some fine precipitates in "1" are Ti-rich, which might be nano TiN. Feature "2" in Fig. 7 denotes the TiN islands which have a triangular-like shape.

Figure 8 shows the microstructure at the tip of the penetration depth of TiN. It is clear to see that the γ' phases ("2"), degrades to Ti-rich nano precipitates ("4") and Al-rich phase ("3"). The TiN formed as shown by "5" has a needle-like shape. Fig. 9 is the EDS mapping results of Fig. 8.

3.2. Simulation results

The simulation results are shown in Fig. 10 with comparison with the experimental data. The experimental data is from Fig. 5b. Four zones are divided based on the experimental microstructures. The surface Cr-oxidation occurs in zone I, the internal oxidation/nitridation of Al is in zone I+II, the internal nitridation of Ti happens in zone I+II+III, zone IV is for $\gamma + \gamma'$ without internal oxidation or nitridation. Since the model focuses on the diffusion of alloying elements (no oxygen and nitrogen) in γ and γ'

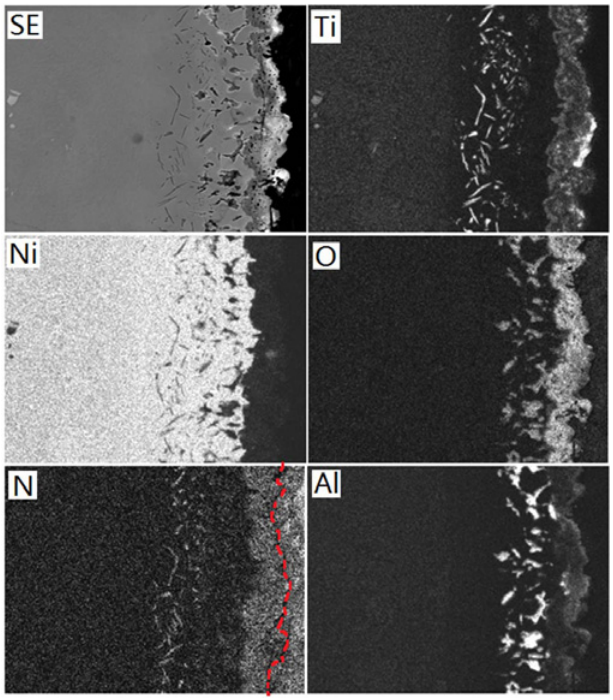

Figure 4. EDS maps of elements for the red square in Fig. 3a.

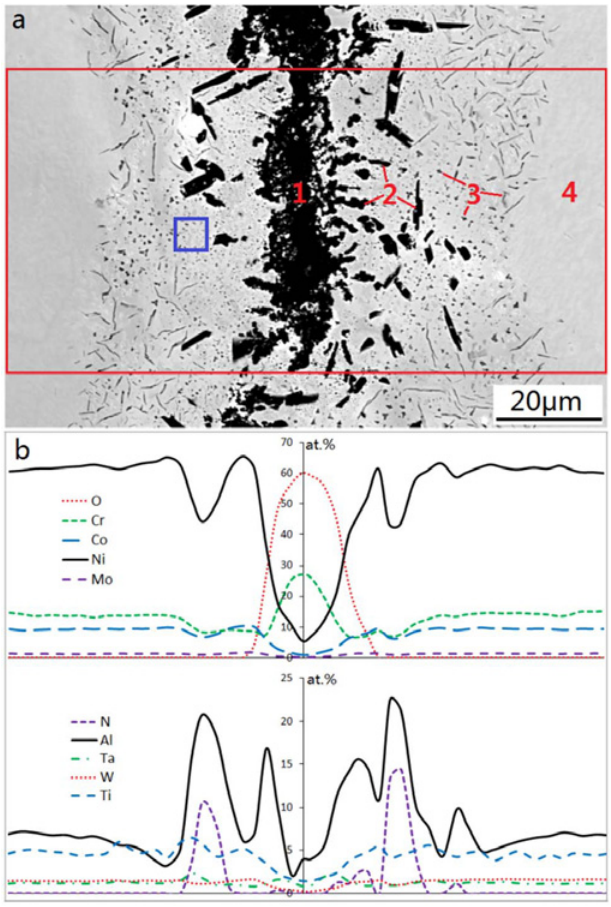

Figure 5. Cracking oxidation. (a) A SEM image showing a crack in the superalloy ("1" for Cr-rich oxides along the crack, "2" for Al_2O_3 and AlN, "3" for TiN, and "4" for $\gamma + \gamma'$). (b) The EDS composition profiles of elements in the red square in figure (a).

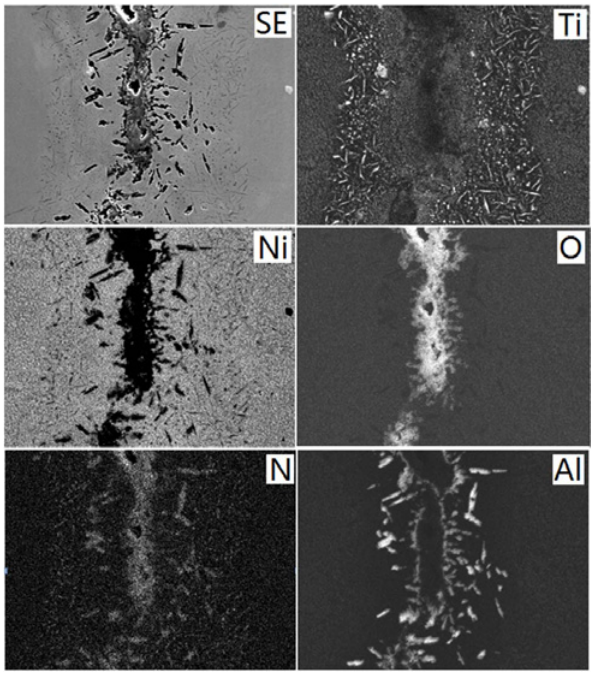

Figure 6. EDS maps of elements for the red square in Fig. 5a.

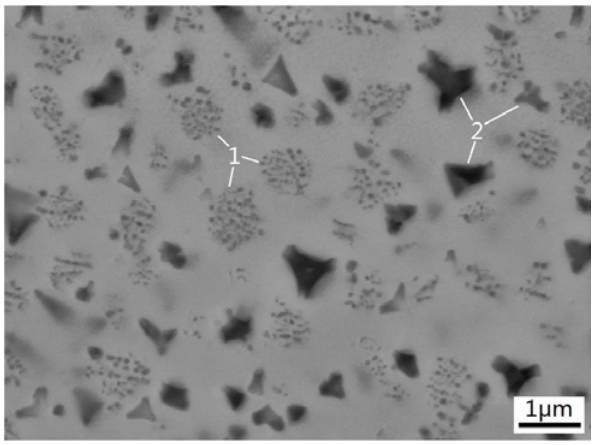

Figure 7. SEM image in the blue square in Fig. 1a. "1" for Ti-rich nano precipitates tracking the previous γ' phase, and "2" for TiN with a triangular-kind shape.

phases, the measured compositions, except in zone I, have been re-normalized with removing the oxygen/nitrogen contents and the oxidized/nitridized Al and Ti contents from the profiles. As shown in Fig. 10a, the simulation agrees well with the experimental results. The profiles of the alloying elements are very well captured. For instance, the surface oxidation of Cr decreases the Cr content in zone II, and the internal oxidation/nitridation makes the Al and Ti contents low in zone II and III. Other elements like Ni and Co become richer in the alloy in zone II and III. The simulated γ' volume profile is given in Fig. 10b. In zone II the total disappearance of γ' is well agreed by the microstructure in Fig. 7 while the partial γ' depletion in zone III is also comparable with the result in Fig. 8.

One disagreement between the simulation and experiment is the Al content in zone II; the model predicts ~4% of Al but the experimental Al content is ~0.5%. This could

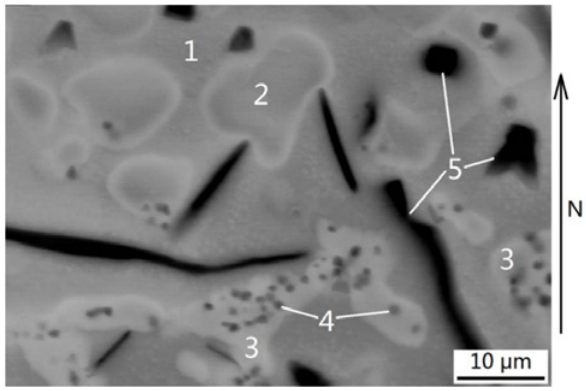

Figure 8. SEM image showing the internal nitridation of Ti and the degradation of γ' phases in the superalloy (the arrow shows the diffusing direction of N). "1" for γ matrix phase, "2" for γ' phase, "3" for decomposing Al-rich, Ti-lack γ' phase, "4" for nano Ti-rich precipitate in "3", and "5" for TiN.

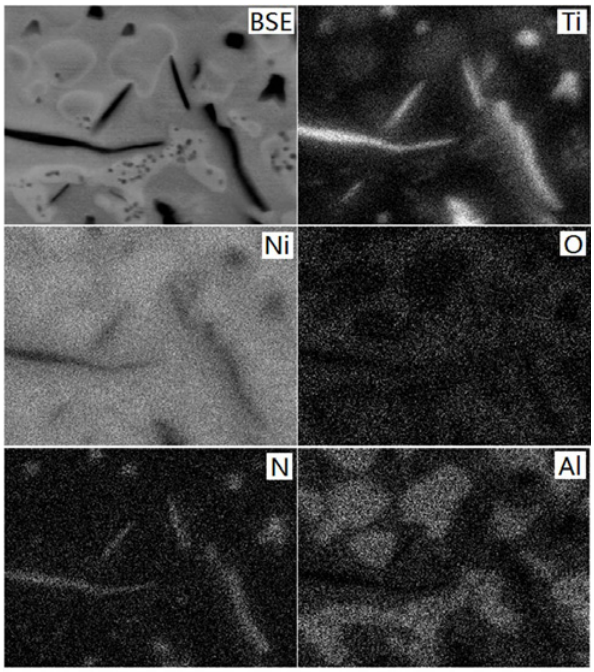

Figure 9. EDS maps of elements for Fig. 8. Note that the "richness" of O in γ matrix is fake due to the overlap of the energy peaks of O with Cr.

be due the over-estimation of the oxidation time; the total creep time 680 h is used in the simulation but the crack and the cracking oxidation may occur in a short time at the end of the testing.

4. Discussions

As shown in Fig. 3 and Fig. 5, the oxidation and nitridation occurred at the sample surface and along the cracking surfaces. Cr-oxides formed as a surface layer and were porous, while oxides and nitrides of Al and/or Ti were only shown as internal precipitates. One interesting phenomenon is that AlN was observed under the cracking surfaces but was not found in the sample-surface oxidation situation. This could be explained by that the solution of

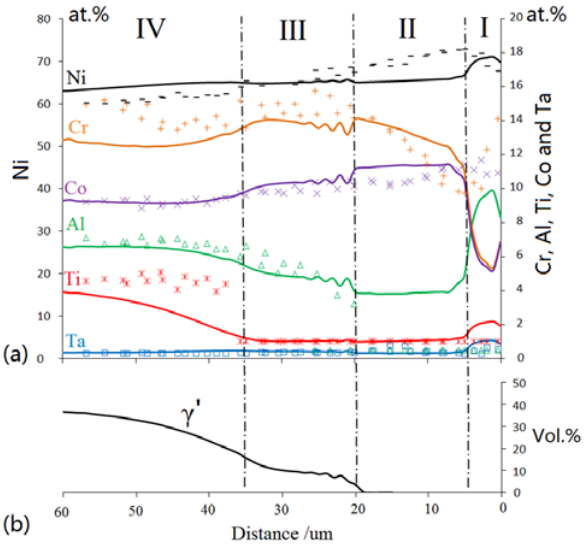

Figure 10. Modelling results of (a) the alloying composition profiles (by atomic%) and (b) the γ' profile (by volume%, with balance of γ) for the cracking oxidation in the superalloy IN-792 after the oxidation/nitridation at 900 ° C for 680 h. Distance=0 denotes the surface. Four zones are marked in the graph: zone I mainly containing Cr_2O_3, zone II containing Al_2O_3 +AlN +TiN, zone III containing TiN, and zone IV containing none internal oxides/nitrides. The points are the experimental results from Fig. 5b; note that the experimental compositions in the penetration depth of internal oxidation and nitridation of Al (I+II) and Ti (I+II+III) have been recalculated by removing oxygen and nitrogen content and the oxidized and nitridized content of Al and Ti.

oxygen under the cracking surfaces was low, due to the larger consumption of the external oxidation of Cr on the sample surface and along the crack. Then the un-oxidized Al in the alloy could be nitridized. Ti was only nitridized, indicating the higher thermodynamic stability of TiN than that of Ti-oxides.

The following discussion will mainly focus on the oxidation/nitridation happening at cracks, by considering that in real applications superalloys are always protected by protective coatings which lowers the possibility of the occurrence of the direction oxidation on the superalloy surface. However the oxidation and nitridation occurring at cracks are still interesting, because cracking oxidation can still a problem if the coating is cracked with the crack penetrating into the superalloy.

4.1. Penetration depth of internal oxides/nitrides

The thermodynamic explanation for the different penetration depths of the different precipitates is their different free energy of the formation [2]. However, kinetically, the penetration depth of oxides/nitrides should be related to the diffusion of oxygen, nitrogen and the alloying elements.

In the cracking oxidation case in the superalloy IN-792, three different precipitates, i.e. Al_2O_3, AlN and TiN, are formed internally and show different penetration depths, as shown in Fig. 5. The penetration depth of those precipitates can be simply calculated by using the classical internal-oxidation theory by Wagner [5]. For instance, the penetration depth of Al_2O_3 precipitates, X, can be expressed as follows [12], by assuming that the solute diffusion of Al is very slow relative to that of oxygen, and the oxygen solubility is very small relative to that of Al ($c_O^s = 3.72 \times 10^{-2}\, at.\%$ (calculated by [13]) $\ll c_{Al}^0 = 7.29\, at.\%$ in IN792).

$$X = \left[\frac{2c_O^s D_O}{\nu c_{Al}^0} t\right]^{1/2} \quad (1)$$

where c_O^s denotes the surface soluble concentration of oxygen, D_O s the oxygen diffusivity, ν is chemical stoichiometric coefficient of the precipitate in a form of MO_ν($\nu = 1.5$ for Al_2O_3, $\nu = 1$ for AlN and TiN), c_{Al}^0 is the original concentration of the solute element in the alloy, and t is time.

The diffusion coefficient and solubility of oxygen and nitrogen in IN-792 are known. By using values found in the literature for pure Ni or Ni-Cr alloys: $c_O^s = 3.72 \times 10^{-2}\, at.\%$ [12], $D_O = 4.85 \times 10^{-13}\, m^2/s$ [12], $c_N^s = 1.8 \times 10^{-3}\, at.\%$ [2], and $D_N = 1.95 \times 10^{-11}\, m^2/s$ [2], the penetration depth of nitride and oxides in the investigated IN-792 specimen was estimated by Eq. (1). The calculated penetration depths are $X_{Al_2O_3}$ =90 μm, $X_{AlN} = 154\,\mu$m and $X_{TiN} = 188\,\mu$m, respectively, which are larger than the experimental values (in Fig. 5, $X_{Al_2O_3} =\sim 5$–$10\,\mu$m, $X_{AlN} =\sim 15$–$25\,\mu$m, and $X_{TiN} =\sim 30$–$40\,\mu$m, respectively). The mismatch between the calculation and experimental results could be related to: errors due to the use of diffusivity of oxygen and nitrogen for Ni or Ni-Cr alloy, the applicability of Eq. (1) when two or more oxides or nitrides are formed simultaneously [6], and neglecting possible influence of the diffusion of the alloying elements. Nevertheless, the order of penetration depth predicted by the simple calculation fits well to the experimental results, i.e. $X_{TiN} > X_{AlN} > X_{Al_2O_3}$.

Since the calculation by Eq. (1) can not predict the penetration depth of the internal oxides and nitrides quantitatively, the oxidation-diffusion model (Fig. 1) only uses the experimentally-measured values as input.

4.2. Microstructure degradation

Since the Cr-rich oxide along the crack in Fig. 5 is porous, oxygen and nitrogen can easily diffuse into the superalloy matrix, resulting in internal oxidation and nitridation [2,3]. By removing the oxidized and nitridized Cr, Al Ti in zone I, II and/or III in the model, to simulate the oxidation and nitridation, the elemental activity in metallic phases (γ/ γ') in the alloy is changed locally, which drives the homogenization diffusion of the alloying elements through the superalloy. The changes of the elemental profiles also cause the microstructure degradation, e.g. that the decreased concentration of Al and Ti in zone II and III destabilizes γ'. According to the results in Fig. 10b, (Al,Ti)-rich γ' phase is completely disappeared from zone II, which agrees well with the microstructure shown in Fig. 7, i.e. that Ti and Al in previous γ' phases have been totally oxidized or nitridized in this zone. In zone III the existence of $\gamma'$is predicted by the model which is due to the high enough content of Al in this zone to support the

formation of γ', that agrees well with the microstructures in Figs. 8, 9 where γ' is decomposing but still remained in an Al-rich form. The oxidation and nitridation of Cr, Al and Ni also cause a change of the profiles of other alloying elements like Ni, Co and Ta, which shows a good agreement of the results between the simulation and the experiment (Fig. 10a).

So far the model has to use the experimental data, i.e. by measuring the oxidized and nitridized content of Cr, Al and/or Ti, as the input for the microstructural evolution simulation. The main reason, as discussed in Section 4.1, is the lack of data of the solubility and diffusivity of oxygen and nitrogen in alloys. In addition, the thermodynamic data in oxide-alloy system, for instance the formation and dissolution of oxides as precipitates in alloys, is still unwell built. However, the model developed in this paper has shown the good capacity for the use to simulate the microstructural evolution in an oxidation and nitridation environment, and can be applicable in the future with more accurate diffusion data of oxygen/nitrogen being developed.

5. Conclusion

The microstructures in a creep superalloy of IN-792 have been analysed at 950 $^\circ$ C. An oxidation-diffusion model was developed to simulate the alloying element diffusion and the microstructural evolution in the superalloy, by integrating the surface and internal oxidation and nitridation. Some main conclusions can be obtained as follows:

- Internal oxidation and nitridation are found under the outside Cr-oxide layer which is porous and even cracked in the superalloy. Internal Al_2O_3 and TiN precipitates are formed in the oxidation at sample surface, while, besides Al_2O_3 and TiN, AlN is also detected in the oxidation along the cracking surfaces.
- The order of the penetration depths of the internal oxides and nitrides is $TiN > AlN > Al_2O_3$ in the superalloy under the oxidized crack. Wagner's theory is tested to quantitatively calculate the penetration depths, but fails to predict the exact values from the experimental measurement.
- The oxidation-diffusion model predicts well the alloying diffusion and the γ' depletion in the superalloy, by taking the oxidation and/or nitridation of Cr, Al and Ti into account. It is found that the outside oxidation of Cr decreases the Cr concentration in the metallic matrix under the Cr-oxide layer. The concentration of Al (Ti) is also very low (near to zero) in the metallic matrix where Al (Ti) is oxidized and/or nitridized internally.
- The model built in this paper can be more useful in the future with more accurate diffusion data of oxygen and nitrogen being developed.

The Siemens Industrial Turbomachinery AB (Finspång, Sweden) and Swedish Energy Agency through KME consortium – ELFORSK are greatly acknowledged for their financial support in this research.

References

[1] J. Litz, A. Rahmel, M. Schorr, Oxidation Metals **30**, 1 (1987)
[2] U. Krupp and H.J. Christ, Metall. Mater. Trans. A **31A**, 1 (2000)
[3] F. Abe, H. Araki, H. Yoshida, M. Okada, Oxidation Metals **27**, 1 (1987)
[4] R. Rubly and D. Douglass, Oxidation Metals **35**, 3 (1991)
[5] C. Wagner, Zeitschrift für Elektrochemie, Berichte der Bunsengesellschaft für physikalische Chemie **63**, 7 (1959)
[6] U. Krupp and H. Christ, Oxidation Metals **52**, 3 (1999)
[7] H. Larsson and A. Engström, Acta Mater. **54**, 9 (2006)
[8] J.M. Larson, Metall.Trans.A **7A**, 10 (1976)
[9] H. Larsson and R.C. Reed, Acta Mater. **5**6, 15 (2008)
[10] J. Agren, J. Phys. Chem. Solids **43**, 4 (1982)
[11] Thermo-Calc Software AB, (2008)
[12] N. Birks, G.H. Meier, F.S. Pettit, Cambridge University Press, POB 110, Cambridge, CB2 3RL, UK, [URL:http://www.cambridge.org.lt.ltag.bibl.liu.se/], (2006)
[13] J. Park and C.J. Altstetter, Metallurgical Transactions A **18**, 1 (1987)